Liraglutide improves adipose tissue remodeling and mitochondrial dynamics in a visceral obesity model induced by a high-fat diet

Vanessa Touceda [a,b], Florencia Fontana Estevez [a], Leonardo Cacciagiú [b,c], Paola Finocchietto [d], Romina Bustos [a], Agustina Vidal [a], Gabriela Berg [e], Celina Morales [f], Germán González [a], Veronica Miksztowicz [a,b,*]

[a] Pontificia Universidad Católica Argentina. Facultad de Medicina, Instituto de Investigaciones Biomédicas (UCA-CONICET), Laboratorio de Patología Cardiovascular Experimental e Hipertensión Arterial, Buenos Aires, Argentina
[b] Universidad de Buenos Aires, Facultad de Odontología, Cátedra de Bioquímica General y Bucal, Buenos Aires, Argentina
[c] Hospital General de Agudos Teodoro Álvarez, Laboratorio Central, Sección Bioquímica, Buenos Aires, Argentina
[d] Universidad de Buenos Aires, Facultad de Medicina. Instituto de Inmunología, Genética y Metabolismo (INIGEM. UBA-CONICET), Laboratorio de Metabolismo del Oxígeno, Buenos Aires, Argentina
[e] Universidad de Buenos Aires, Facultad de Farmacia y Bioquímica, Departamento de Bioquímica Clínica, Laboratorio de Lípidos y Aterosclerosis, Buenos Aires, Argentina
[f] Universidad de Buenos Aires, Facultad de Medicina, Departamento de Patología, Buenos Aires, Argentina

ARTICLE INFO

ABSTRACT

Central obesity is characterized by visceral adipose tissue (VAT) expansion, considered one of the main risk factors for metabolic complications. In recent years, new drugs have been studied for obesity treatment. Liraglutide (LGT), a GLP-1 agonist, decreases body weight, however, several mechanisms of action on VAT are still unknown.

Aim: to study the effect of LGT on factors associated with VAT remodeling and mitochondrial dynamics in mice fed a high-fat diet (HFD).

Methods: C57BL/6 mice were divided into Control (C) and HFD. After 15 weeks of feeding, each group was subdivided according to LGT administration for 5 weeks: C, C + LGT, HFD, and HFD + LGT. In epididymal AT (EAT) we evaluated histological and mitochondrial characteristics, vascularity, gelatinase activity (MMPs), and galectin-3 expression.

Results: HFD presented larger adipocytes (p < 0.05), and lower vascular density and MMP-9 activity (p < 0.01) than C, while a major number of smaller adipocytes (p < 0.05) and an increase in vascularity (p < 0.001) and MMP-9 activity (p < 0.01) was observed in HFD + LGT. Collagen content was higher (p < 0.05) in EAT from HFD and decreased in HFD + LGT. In C, C + LGT, and HFD + LGT, mitochondria were predominantly tubular-shaped while in HFD mitochondria were mostly spherical (p < 0.001).

Conclusion: LGT positively influences VAT behavior by modulating gelatinase activity, enhancing vascularization, and improving adipocyte histological characteristics. Additionally, LGT improves mitochondrial dynamics, a process that would favor VAT functionality.

1. Introduction

Visceral adipose tissue (VAT), a fat mass located around internal organs, is considered an independent risk factor for cardiovascular and metabolic diseases. The expansion of VAT leads to central obesity, which is not always reflected in total body weight gain (Sahakyan et al., 2015; Piché et al., 2020; Powell-Wiley et al., 2021).

Since obesity has become a worldwide epidemic, in recent years several therapeutic options have been studied (Milano et al., 2020). Liraglutide (LGT) is a long-acting glucagon-like peptide (GLP)-1 receptor agonist (GLP-1 RA) that is used for the treatment of type 2 diabetes mellitus. LGT promotes a reduction in blood glucose levels by inducing insulin secretion, slowing gastric emptying, and decreasing food intake (Nauck et al., 2021). In 2015, the Food and Drug Administration (FDA)

approved LGT for the treatment of obesity, given the strong evidence of its ability to reduce body weight (Iepsen et al., 2015). However, there are still unknown mechanisms of action on adipose tissue remodeling.

VAT is an active endocrine tissue that regulates the morphology and function of different organs through adipocytokines secretion. The physiological expansion of VAT involves adipogenesis and angiogenesis processes, and both require highly regulated extracellular matrix (ECM) remodeling (Berg et al., 2019). In obesity, the expansion of visceral fat is characterized by a rapid increase in fat cell size (hypertrophy) and/or fat cell number (hyperplasia), leading to VAT dysfunctionality. In addition, the plasticity and expansion of AT are related to its angiogenic capacities, depending on the balance between proangiogenic and anti-angiogenic processes. In expanded VAT, vascularization is affected, and the lack of vessels produces a decrease in oxygen supply in adipocytes, leading to hypoxia and inflammation (Herold and Kalucka, 2021). The angiogenesis process is influenced by different factors, with metalloproteinases (MMPs) being one of the key players (Berg et al., 2014). MMPs are a family of endopeptidases responsible for the degradation of ECM components; they have several regulatory mechanisms essential for tissue homeostasis. (Berg et al., 2019). According to previous studies, we have described that gelatinases MMP-2 and -9 are involved in the angiogenesis process and that their behavior is altered in insulin resistance or obesity (Miksztowicz et al., 2008, 2014; Tinahones et al., 2012; Levi et al., 2022).

Regarding adipogenesis, galectin-3 (Gal-3) has recently emerged as a new adipogenic factor. Gal-3, a β-galactosidase-binding lectin, modulates different biological functions and it is expressed by different cell types such as immune cells, epithelial cells, and adipocytes, among others. Gal-3 regulates inflammation, cell-cell and cell-matrix interactions, and tissue repair (Li et al., 2020b). Gal-3 has also been involved in the pathogenesis of cancer, and inflammatory, cardiovascular, and metabolic diseases (Cassaglia et al., 2020; Li et al., 2020b). Numerous studies have suggested the key function of Gal-3 in VAT maturation and glucose homeostasis (Pang et al., 2013; Pejnovic et al., 2013; Blasetti Fantauzzi et al., 2020); however, its role in VAT pathophysiological expansion is still controversial, and the effect of LGT is unknown.

Finally, evidence suggests an association between tissue remodeling and mitochondria (De Cavanagh et al., 2009). Since mitochondria are dynamic organelles, changes in their structure, function, and cellular distribution affect metabolism. It has been suggested that VAT expansion alters mitochondrial behavior. Different studies reported that adipocyte enlargement is associated with a reduction in mitochondrial oxidative activity and, therefore, they accumulate more lipids leading to further VAT expansion (Li et al., 2017). In obesity, downregulation of mitochondrial biogenesis and an increase in reactive oxygen species production were also observed (Heinonen et al., 2020).

We aimed to investigate the effect of LGT on factors associated with tissue remodeling and mitochondrial dynamics in expanded VAT. To achieve this goal, we evaluated histological characteristics, vascularity, gelatinase activity, Gal-3 expression, and mitochondrial features in VAT from a visceral obesity model induced by a high-fat diet.

2. Materials and methods

2.1. Animal model

In this study we used 8-week-old male C57BL/6 mice obtained from our Bioresources facilities at the Biomedical Research Institute (BIOMED, UCA- CONICET) of the Pontificia Universidad Católica Argentina.

Mice were housed 4–6 per cage with free access to food and drinking water and maintained under controlled temperature (20-22 °C), humidity, and airflow conditions with a fixed 12-h light: dark cycle set.

At 8 weeks of age, animals were randomly divided into two groups and fed for 20 weeks as follows: Control group (C, n = 15) fed with standard chow (197 kcal per 100 g) and High Fat Diet group (HFD, n =

13) fed with a diet containing 40% of the total calories from fat. HFD was prepared as previously described (Barchuk et al., 2018) by adding lard (16% w/w) and high oleic sunflower oil (2% w/w) to provide 250 kcal per 100 g. After 15 weeks, each group was subdivided according to the subcutaneous administration of Liraglutide (LGT, 200 μg/kg/day - Victoza° Novo Nordisk Pharma) or saline solution (equivalent volume) for 5 weeks: C (n = 8), C + LGT, (n = 7), HFD (n = 6) and HFD + LGT (n = 7). The dose and time for LGT treatment were chosen from literature (Tamura et al., 2015; Liu et al., 2021) Body weight, food, and caloric intake were registered weekly throughout the experimental period. Food efficiency ratio (FER) was calculated for each diet according to the following formula:

$$FER\ (\%) = \frac{Total\ weight\ gain\ (g)}{Total\ food\ intake\ (g)}\ x\ 100$$

The experimental protocol (N° 002/2020) was approved by the Institutional Committee for the Care and Use of Laboratory Animals (CICUAL) of BIOMED (UCA-CONICET) in line with the NIH's Guide for the Care and Use of Laboratory Animals (National Research Council, 2012).

2.2. Systolic blood pressure

Systolic blood pressure (SBP, mmHg) was evaluated at the beginning of the experience (basal), before LGT treatment (at week 15), and at the end of the protocol (at week 20). Briefly, the animals were trained for one week before the measurement of SBP by plethysmography according to the tail-cuff method (González et al., 2016). SBP values were registered for three consecutive days each time in a quiet environment and avoiding stressful conditions for the animals. The results of the three measurements were averaged and a single SBP value was considered for each animal.

2.3. Sample collection

At the end of the experimental period, after 4 h of fasting, animals were euthanized with an overdose of sodium pentobarbital (i.p, 150 mg/kg). Blood samples were collected and centrifuged at 950 g for 10 min; serum was obtained and kept at −20 °C for further determination of glycemia and lipid profile. As representative of visceral fat, epididymal adipose tissue (EAT) was removed, weighed, fractionated, and stored in liquid nitrogen for molecular determinations; one fraction of tissue was fixed in 4% formalin buffer, pH 7.0 and conserved at 4 °C for histological evaluation. Another fraction was immediately fixed in a solution of 4% paraformaldehyde, 2% glutaraldehyde, and 5% sucrose in phosphate-buffered saline for evaluation of mitochondrial characteristics by transmission electron microscopy (TEM). The tibia was removed and measured. EAT weight was normalized to tibia length through the following formula: EAT mass (mg)/tibia length (mm).

2.4. Biochemical determinations

Serum glucose, total cholesterol (T-chol), HDL-chol, and triglycerides (TG) were determined by enzymatic colorimetric methods in a Cobas-501 autoanalyzer (Roche Diagnostics, Mannheim, Germany). Non-HDL chol was calculated as the difference between T-chol and HDL-chol as representative of atherogenic lipoprotein levels (Miksztowicz et al., 2014; Raja et al., 2023).

2.5. Histological analysis

For histological analysis, fixed EAT samples were dehydrated in ethanol, and 5 μm paraffin-embedded slices were obtained with a microtome Reichert (Austria). The slices were stained with hematoxylin-eosin reagent and periodic acid-schiff (PAS) stain to quantify size (um²), number of adipocytes (number of adipocytes/mm²), and vascular

density (number of vessels/mm²). Blood vessel density was normalized by adipocyte number. As previously described, elements (adipocytes and blood vessels) were counted in each field and then transformed into cells/mm² or blood vessels/mm² (Miksztowicz et al., 2014, 2017; Maughan et al., 2016), according to the following formula:

$$\text{Element number}\Big/ mm^2 = \frac{\text{Element number per field}}{\text{Field area }(\mu m^2)} \, x \, 1000000 \, \mu m^2/mm^2$$

Histological characteristics were blindly evaluated by a single operator. Quantification was performed by light microscopy in a high-power field at 400x, in 20 fields from different locations of the same tissue section for each animal. Images were analyzed using a computerized image analyzer software (Image ProPlus Version 6.0, Media Cybernetics Corp).

2.6. Fluorescence assay

To evaluate vascular density in EAT a fluorescence assay was also performed. Paraffin-embedded slices of EAT samples were dewaxed with xylene and ethanol. The slices were incubated with a neuraminidase solution (3.3 U/mL, N2876, Merck KGaA) for 1 h at room temperature. Then, sections were incubated with Rhodamine labeled GSL lectin (0.12 mg/mL, Cat# RL-1102, Vector Laboratories) to visualize cell membranes and Fluorescein peanut agglutinin lectin (0.01 mg/mL, Cat# FL-1071, Vector Laboratories) to analyze interstitial tissue, for 2 h at room temperature. Nuclei were stained with DAPI (Vectashield® Cat# H-1200-10, Vector Laboratories). Blood vessels in representative EAT samples were quantified in a confocal microscope in a high-power field at 400x (Zeiss LSM 980, Zeiss) and images were analyzed using a computerized image analyzer software (Image ProPlus Version 6.0, Media Cybernetics Corp).

2.7. Gelatinolytic zymography

MMP-2 and -9 activity was measured by gelatinolytic zymography as previously described (Kleiner and Stetler-Stevenson, 1994). Briefly, an EAT fraction was homogenized in 50 mmol/L Tris buffer, pH 7.4, containing $CaCl_2$ mM, $ZnCl_2$ 1 mM, and Triton X-100 1%. Thirty milligrams of protein from homogenate were loaded in 7.5% polyacrylamide gel copolymerized with gelatin 0.1% (G1890-100G, Merck KGaA) in non-reducing conditions. Gels were run for 1.45 h in 25 mM Tris, 192 mM glycine, 0.1% SDS buffer pH 8.3 at 4 °C, in a Mini Protean® Tetra Cell (Cat #1658005, Bio-Rad Laboratories). After running, gels were rinsed with 2.5% Triton X-100 for 30 min and incubated in 0.15 mol/L NaCl, 10 mmol/L $CaCl_2$, Tris HCl, pH 7.4 at 37 °C overnight. The gels were stained with Coomassie Brilliant Blue R-250 0.25% (Cat #1610400, Bio-Rad Laboratories) and decolorized with acetic acid-methanol-water (1:3:6). Enzyme activity was detected as colorless bands against the blue-stained background. MMP-9 (84 kDa) and MMP-2 (67 kDa) were identified by molecular weight. Precision Plus Protein Dual Color Standards (Cat #1610374, Bio-Rad Laboratories) was used as the protein molecular weight standard and conditioned media from fibroblasts was used as an activity standard. Band intensities were quantified by densitometric analysis using the Fluorchem software (Alpha Innotech Corp), and relative activity was expressed as a ratio to the standard.

2.8. Interstitial collagen

Interstitial collagen was evaluated in paraffin-embedded slices stained with Picrosirius red. The percentage of collagen for each region was measured and expressed as collagen volume fraction (%, collagen area/tissue area). Quantification was performed by light microscopy in a high-power field at 400x, in 10 fields from different locations of the same tissue section for each animal. Images were evaluated by a single operator in a blinded manner and analyzed using a computerized image analyzer software (Image ProPlus Version 6.0, Media Cybernetics Corp).

2.9. Western blotting

EAT was homogenized in 20 mmol/L Tris buffer, pH 7.4, containing 150 mmol/L sodium chloride, 1% Triton X-100, and 2% Protease Inhibitor Cocktail (P8340-1 ML, Merck KGaA). Thirty micrograms of protein from each sample were separated in 12% SDS-PAGE, and gels were run for 1.30 h in a Mini Protean® Tetra Cell (Cat #1658005, Bio-Rad Laboratories). After running, gels were electroblotted onto polyvinylidene difluoride membranes (Cat #88518, Thermo Fisher Scientific) using the Mini Trans-Blot® Module (Cat #1703811, Bio-Rad Laboratories) Blots were blocked with 5% skimmed milk for 1 h and incubated overnight at 4 °C with a polyclonal rabbit antibody against Gal-3 (Cat #PB9081, Boster Biological Technology Co.) or polyclonal mouse antibody against UCP-1 (Cat# sc-293,418, RRID: AB_2811175, Santa Cruz Biotechnology) and β-Actin (Cat #PA5-85291, RRID: AB_2792434, Thermo Fisher Scientific) as loading control. Then, blots were incubated with peroxidase-conjugated anti-rabbit antibody (Cat# BA1054–0.5, Boster Biological Technology) for Gal-3 and actin or peroxidase-conjugated anti-mouse antibody (Cat# W402B, Promega Corporation) for UCP-1, for 1.30 h at room temperature. The specific signals were visualized using the Image Quant LAS 4000 luminescent image analyzer (General Electric). Bands were identified using pre-stained molecular weight standard (Cat #1610374, Bio-Rad Laboratories). The relative intensity of the protein signal was quantified by densitometric analysis using the Fluorchem software (Alpha Innotech Corp). Results were expressed as Gal-3/β-Actin and UCP-1/β-Actin protein ratio.

2.10. Transmission electron microscopy

To perform the analysis of mitochondria through transmission electron microscopy (TEM), EAT samples were fractionated in 1 mm² cubes and fixed in 4% paraformaldehyde, 2% glutaraldehyde, and 5% sucrose in phosphate-buffered saline, followed by 2-h post-fixation in 1% osmium tetroxide, and then 1 h in uranyl acetate in 50% ethanol. Samples were washed with 50% ethanol and dehydrated with a graded series of ethanol, clarified with acetone, and embedded in Vestopal. Grids were prepared and stained with uranyl acetate and lead citrate. Samples were observed at 100 kV using a transmission electron microscope (Zeiss EM-109-T, Zeiss). The percentage distribution of tubular and fragmented mitochondria in adipocytes was determined in a minimum of 8–10 random fields at 3.000-30.000× magnification to ensure a representative area of analysis. Mitochondria whose length was more than three times their width were classified as tubular, whereas round mitochondria were considered fragmented.

2.11. Statistical analysis

Data is presented as mean ± SD or median (range) according to normal or skewed distribution, respectively. Differences between groups were analyzed using unpaired Student T test, Anova test or Kruskal Wallis, and Bonferroni or Dunns test a posteriori according to group number and data distribution. Pearson or Spearman analyses, for parametric or non-parametric variables, were used to determine correlations between parameters. Before the analysis of the different variables, the ROUT test was performed to identify outliers. GraphPad Prism 8 software (Prism version 8.0.1, GraphPad) was used for statistical analysis and graphical design. A $p < 0.05$ was considered significant.

3. Results

3.1. General characteristics of the animal model

At week 15 and the end of the experience, body weight, caloric intake, and SBP were similar between groups (Tables 1 and 2, respectively).

EAT mass was significantly higher in HFD compared to C group (p < 0.05). A significant decrease in EAT mass was observed in HFD + LGT in comparison with HFD group, even after tibia length correction (p < 0.001) (Table 2).

3.2. Circulating biochemical parameters

In reference to lipid profile, HFD group presented higher T-chol (p < 0.001) and non-HDL chol (p < 0.05) levels than C. In comparison to HFD, both parameters were decreased in HFD + LGT (p < 0.01 and p < 0.05 respectively). Lower TG levels were observed only in HFD + LGT (p < 0.05 vs HFD). Glycemia was similar between groups (Table 3).

3.3. Histological characteristics

Histological characteristics of EAT were evaluated in hematoxylin-eosin-stained slices. As expected, HFD presented larger adipocytes than C group (p < 0.05), while a major number of smaller adipocytes was observed in HFD + LGT compared to HFD (p < 0.05) (Fig. 1). Adipocyte size was directly associated with glucose (r = 0.403, p = 0.046), T-chol (r = 0.781, p = 0.001), and non-HDL chol (r = 0.513, p = 0.009) levels, whereas adipocyte number was inversely associated with T-chol (r = −0.486, p = 0.012) and non-HDL chol (r = −0.533, p = 0.005).

3.4. Vascular density

At first, vascular density was analyzed in hematoxylin-eosin stained slices. A significant decrease in vascularity was observed in HFD in comparison to C (p < 0.01), and it significantly increased in HFD + LGT in comparison to HFD group (p < 0.001) (Fig. 1). This difference remains significant after normalizing to adipocyte number (HFD vs HFD + LGT p = 0.026). Even more, in HFD + LGT vascular density was significantly higher than C group (p < 0.01). Finally, vascular density was inversely associated with glucose (r = −0.457, p = 0.022), T-chol (r = −0.519, p = 0.008), and adipocyte size (r = −0.589, p = 0.002) and directly correlated with adipocyte number (r = 0.568, p = 0.003).

To confirm the differences in vascular density between groups with a more specific method, a fluorescence assay was performed. HFD presented lower vascular density than C group (p < 0.05), while with LGT treatment an increase was observed (p < 0.001 vs HFD) (Fig. 2).

3.5. Gelatinolytic activity

In the HFD group, MMP-9 activity was detected only in 3 animals,

Table 1
General characteristics of the animal model before LGT treatment.

	Control	HFD
Initial body weight (g)	24.0 ± 1.3	24.5 ± 1.2
Pre- treatment weight (g)	30.7 ± 1.5	31.2 ± 2.6
Weight gain (g)	6.7 ± 1.0	6.8 ± 1.8
Caloric intake weeks 1–8 (kcal/day/100 g b.w.)	45 ± 4	33 ± 4
Caloric intake weeks 9–15 (kcal/day/100 g b.w.)	37 ± 2	33 ± 1
Food consumption weeks 1–8 (g/day/100 g b.w.)	25 ± 4	16 ± 2
Food consumption weeks 9–15 (g/day/100 g b.w.)	20 ± 1	16 ± 1
Systolic blood pressure (mmHg)	112 ± 13	108 ± 9

Data are expressed as Mean ± SD. HFD: High Fat Diet b.w.: body weight. Student T test.

Table 2
General characteristics of the animal model at the end of the experience.

	Control	Control + LGT	HFD	HFD + LGT
Final body weight (g)	31.5 ± 0.7	30.4 ± 1.0	31.6 ± 1.7	31.5 ± 1.1
Weight gain (g)	−0.4 ± 1.5	−0.3 ± 1.4	0.6 ± 1.0	−0.2 ± 1.8
Caloric intake weeks 15–20 (kcal/day/100 g b.w.)	39 ± 4	34 ± 2	29 ± 3	29 ± 2
Food consumption (g/day/100 g b.w.)	21 ± 2	19 ± 3	14 ± 2	14 ± 2
Food efficiency ratio (%)	0.85 (0.55–1.23)	1.04 (0.93–1.05)	1.41 (1.13–1.42)	1.36 (0.88–1.51)
Systolic blood pressure (mmHg)	117 ± 9	103 ± 9	101 ± 6	103 ± 13
EAT mass (mg)	482 ± 88	407 ± 158	843 ± 105[*,a,**,b]	361 ± 180[***,c]
Tibia length (mm)	16.4 ± 0.4	16.2 ± 0.4	16.7 ± 0.7	17.1 ± 0.5
EAT mass/tibia length	29.3 ± 5.0	25.0 ± 9.3	45.6 ± 9.3[*,a,b]	21.3 ± 10.7[***,c]

Data are expressed as Mean ± SD or Median (Range) according to data distribution. LGT: Liraglutide; HFD: High Fat Diet; b.w.: body weight. ANOVA test or Kruskall-Wallis test followed by Bonferroni or Dunns test a posteriori according to group number and data distribution.
*p < 0.05.
***p < 0.001.
[a] Vs Control.
[b] Vs Control + LGT.
[c] Vs HFD.

Table 3
Circulating biochemical parameters of Control and High Fat Diet group with and without Liraglutide treatment.

	Control	Control + LGT	HFD	HFD + LGT
Glucose (mg/dL)	230 ± 34	208 ± 54	239 ± 50	190 ± 48
Triglycerides (mg/dL)	58 ± 10	71 ± 19	56 ± 10	43 ± 8[*,c]
Total cholesterol (mg/dL)	95 ± 5	82 ± 11	125 ± 7[***,a,b]	107 ± 12[**,c]
HDL cholesterol (mg/dL)	77 ± 10	66 ± 13	102 ± 2	89 ± 9
Non-HDL cholesterol (mg/dL)	18 ± 6	16 ± 4	26 ± 4[*,a,b]	17 ± 6[*,c]

Data are expressed as Mean ± SD. LGT: Liraglutide. HFD: High Fat Diet. ANOVA test followed by Bonferroni test a posteriori.
*p < 0.05.
**p < 0.01.
***p < 0.001.
[a] Vs Control.
[b] Vs Control + LGT.
[c] Vs HFD.

and it was decreased in comparison to C (p < 0.01). HFD + LGT group presented a significant increase in enzyme activity in comparison with HFD (p < 0.01) (Fig. 3). Moreover, in HFD + LGT an increase of 32% in activity compared to the C group was observed. MMP-2 activity was similar between groups; and it was directly associated with vascular density (r = 0.555, p = 0.031) and inversely with glucose levels (r = −0.457, p = 0.031).

3.6. Interstitial collagen

Interstitial collagen in EAT was evaluated in Picrosirius red-stained slices. As shown in Fig. 4, EAT from HFD presented higher interstitial

A.
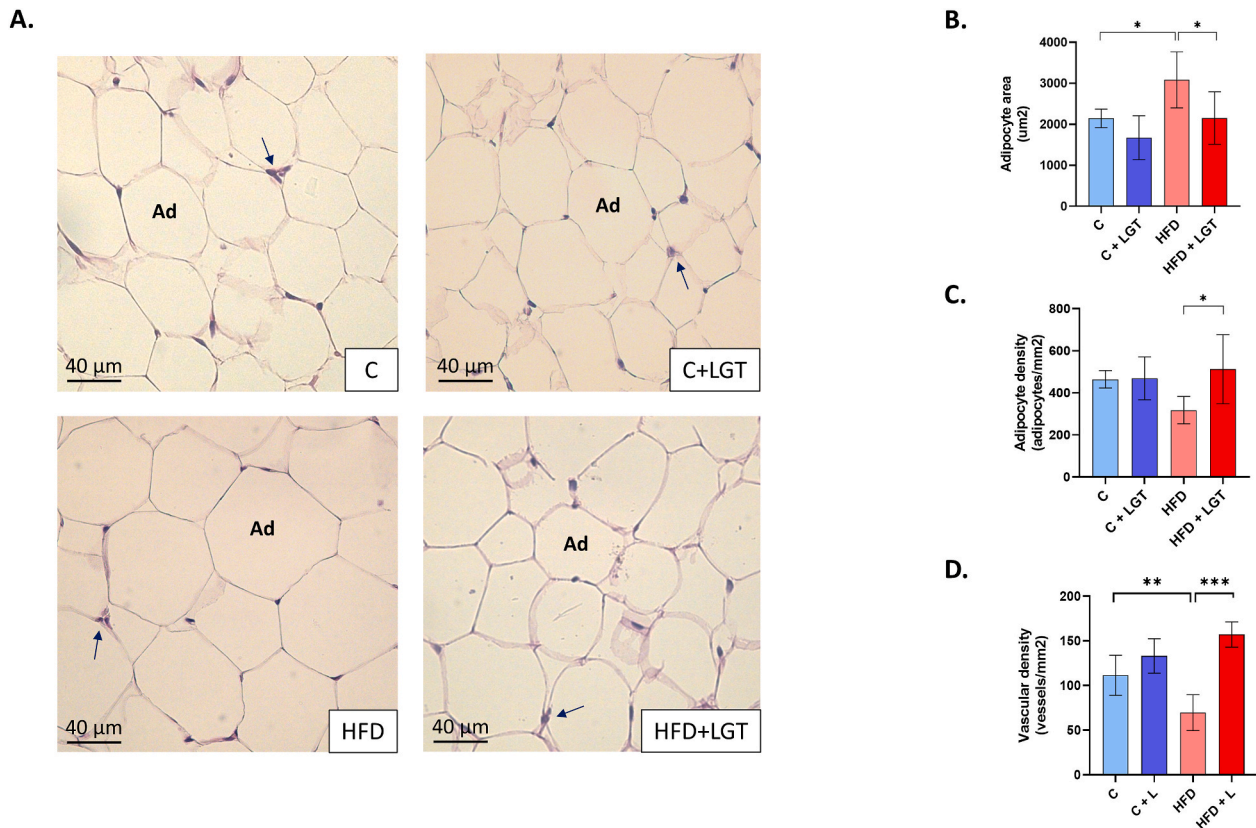
Fig. 1. Analysis of histological characteristics of visceral adipose tissue by hematoxilin-eosin staining. Representative images of H-E-stained sections (A) and histological characteristics of epididymal adipose tissue: adipocyte area (B), adipocyte density (C) and vascular density (D) in Control (C), Control + LGT (C + LGT), HFD and HFD + LGT group. Ad: Adipocytes. Arrows: Blood vessels. Data are presented as mean ± SD. *p < 0.05, **p < 0.01, ***p < 0.001.

collagen content than C group (p < 0.05), and a significant decrease was observed in HFD + LGT (p < 0.05 vs HFD).

3.7. Galectin-3 expression

Gal-3 expression was significantly decreased in HFD and HFD + LGT in comparison to C group (p = 0.01) (Fig. 5). Moreover, Gal-3 levels were negatively associated with adipocyte size (r = −0.625, p = 0.013) and directly correlated with adipocyte number (r = 0.618, p = 0.014). There was no association between Gal-3 and vascular density.

3.8. Mitochondrial morphology and thermogenesis function

Mitochondrial morphology was evaluated by transmission electron microscopy (TEM). In C and C + LGT groups, mitochondria were predominantly tubular-shaped (81 ± 5 and 72 ± 3% respectively), while in the HFD group mitochondria were mostly small and spherical (70 ± 3%), indicating a prevalence of fragmented mitochondria in expanded EAT in comparison with C (p < 0.001). As a result of LGT treatment, EAT from HFD + LGT presented a significant increase in tubular-shaped mitochondria compared to HFD (56 ± 3 vs 30 ± 3%, respectively, p < 0.001) (Fig. 6).

In HFD a decrease in UCP-1 levels was observed in comparison with C group, and LGT administration in HFD favored a recovery in protein expression (Fig. 7).

4. Discussion

In the present study, we investigated the effects of LGT, a GLP-1 agonist, on factors associated with VAT remodeling in a visceral obesity model induced by a high-fat diet. To our knowledge, this is the first time that the effects of LGT on gelatinases activity, as an angiogenic factor, and Gal-3, as an adipogenic factor in expanded VAT, have been reported. We found that LGT treatment promotes: 1) an improvement in atherogenic lipoprotein profile, indicated by non-HDL cholesterol levels; 2) a significant decrease in VAT mass together with an increase in smaller adipocytes number; 3) an increase in vascularity accompanied by an increase in gelatinase activity, especially MMP-9; 4) a decrease in interstitial collagen content; 5) a negative effect of HFD on Gal-3 expression without changes produced by LGT; 6) a prevalence of tubular shaped mitochondria and elevated UCP-1 levels. Our results suggest that in visceral obesity, the decrease in fat mass and the higher number of small adipocytes generated by LGT are accompanied by an increase in VAT vascularization, which is probably due to an increase in MMPs activity.

Adipogenesis, angiogenesis, and ECM remodeling are essential and closely related processes involved in VAT development and expansion. In the present study, there were no differences in final body weight and energy intake; however, an increase in visceral fat content was observed in animals fed a HFD. These findings suggest that there was a necessary variation in the diets' energy utilization efficiency, which caused an excess of saturated fat accumulation in adipose tissue. In this study, the Food Efficiency Ratio showed a tendency to be higher in the HFD group than Control leading to adipose tissue expansion and remodeling. Our results are in accordance with previous studies that demonstrated that the composition of a diet may produce changes in energy utilization that lead to excess fat deposition (Brinkworth et al., 2009). Therefore, it is important to consider that mice in different strains show different tendencies to obesity. Li et al. (2020a) reported that strain C57BL/6 fed HFD did not significantly increase in total body weight compared to C57BL/6 fed a standard diet. In our study visceral obesity was confirmed by an increase in epididymal fat mass in animals fed HFD with larger
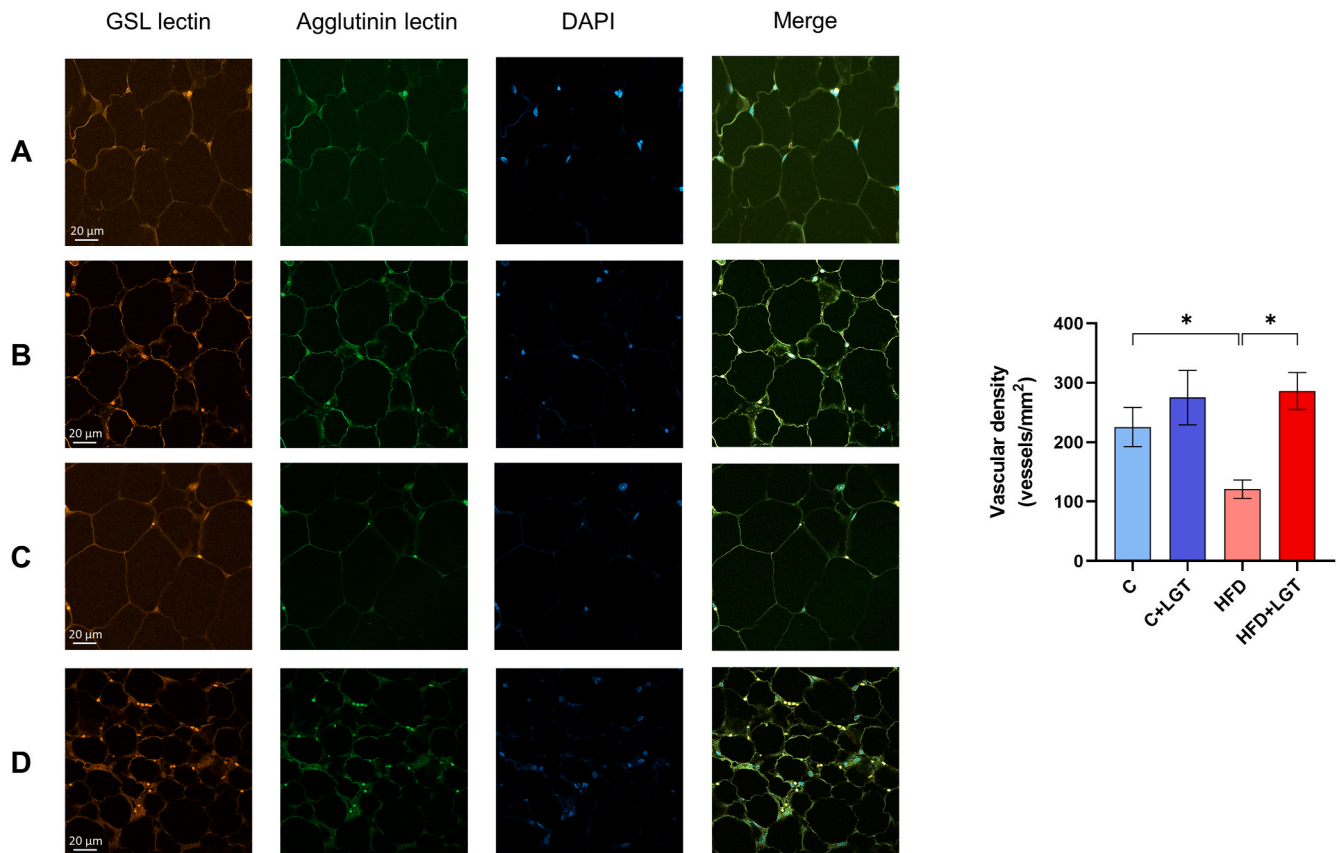
Fig. 2. Evaluation of vascular density in visceral adipose tissue by fluorescence assay. Representative images of rhodamine labeled GSL lectin, fluorescein peanut agglutinin lectin and DAPI stained sections of representative epididymal adipose tissue samples (n = 2 per group, 5 field per sample). Control (A), Control + LGT (B), HFD (C) and HFD + LGT (D) groups. Data are presented as mean ± SD. *p < 0.05.
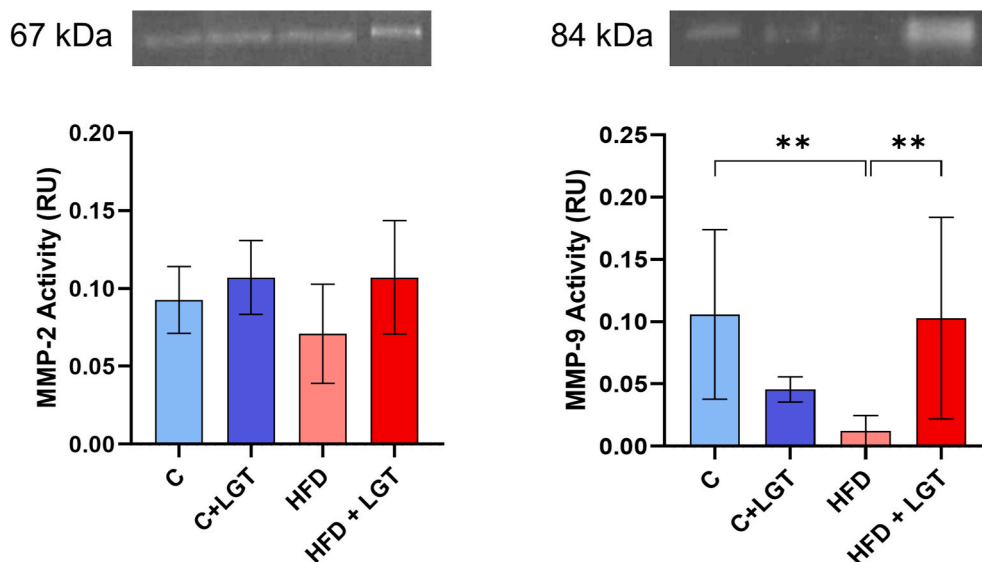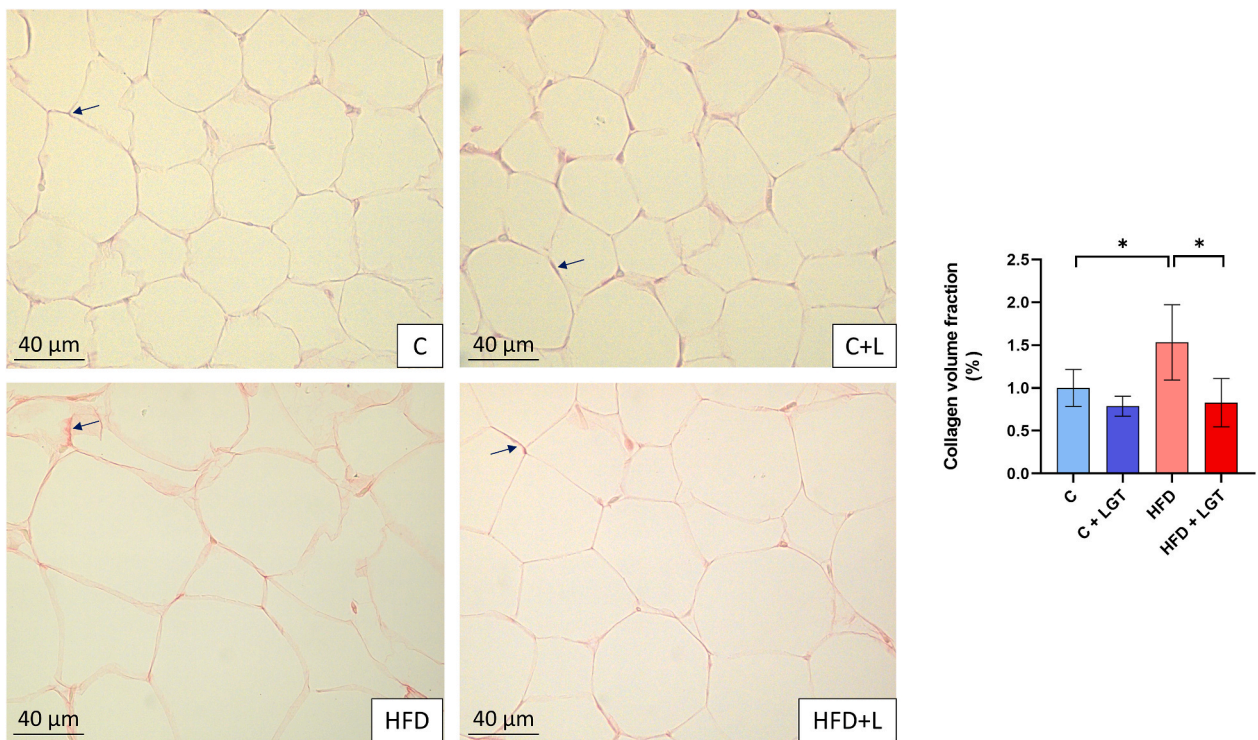

Fig. 3. Gelatinolytic activity evaluation in visceral adipose tissue by zymography. MMP-2 and -9 activity in epididymal adipose tissue from Control (C), Control + LGT (C + LGT), HFD and HFD + LGT group. RU, relative units. Data are presented as mean ± SD. **p < 0.01.

adipocytes and decreased vascular density. We observed that LGT treatment improved the histological characteristics of expanded VAT by decreasing adipocyte size and increasing vascular density, suggesting a beneficial effect of GLP-1 agonists on VAT remodeling.

Gelatinases are proteolytic enzymes that belong to the MMPs family, capable of degrading different components of ECM (Berg et al., 2019).

Numerous studies about MMPs behavior in obesity animal models exist, however, the results remain controversial. These controversies are likely related to the fact that MMPs show different expression patterns depending on age, experimental model, period of experience, diet, and tissue studied. Moreover, MMPs activity is regulated by their specific tissue inhibitors (TIMPs) whose expression pattern is also variable, so

Fig. 4. Measurement of interstitial collagen content in visceral adipose tissue by Picrosirius Red staining. Representative images of Picrosirius Red stained sections and collagen volume fraction (%) quantification in epididymal adipose tissue from Control (C), Control + LGT (C + LGT), HFD and HFD + LGT group. Arrows: Interstitial collagen. Data are presented as mean ± SD. *p < 0.05. (For interpretation of the references to color in this figure legend, the reader is referred to the Web version of this article.)
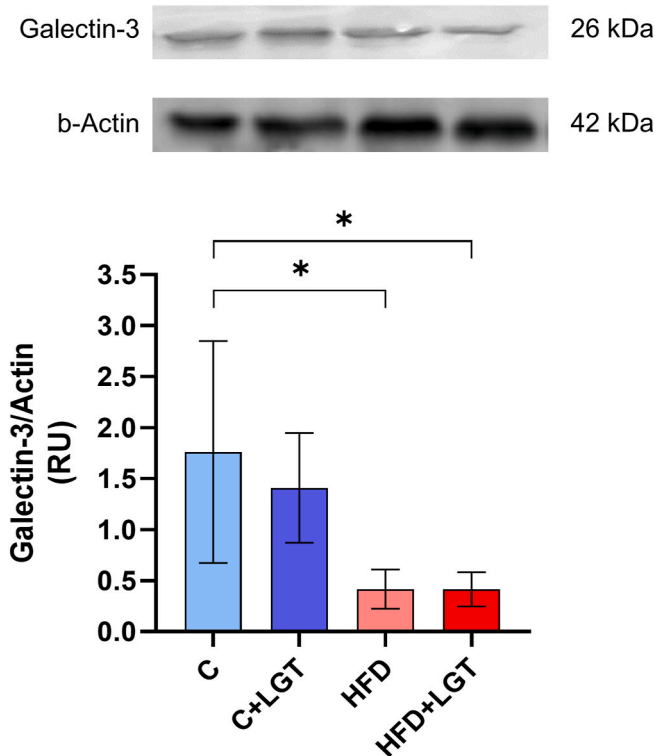
Fig. 5. Quantification of Galectin-3 expression in visceral adipose tissue by western blotting. Galectin-3 levels in epididymal adipose tissue from Control (C), Control + LGT (C + LGT), HFD and HFD + LGT group. RU, relative units. Data are presented as mean ± SD. *p < 0.05.

the final MMPs activity depends on the MMP/TIMPS balance (Berg et al., 2019). Recently, Wołosowicz et al. (2022) reported an increase in MMP-2 and MMP-9 expression in VAT and subcutaneous AT (SAT) in an animal model fed with a HFD for 10 weeks. In contrast, we previously observed a decrease in MMP-2 and MMP-9 levels and activity in VAT from an insulin resistance animal model induced by a sucrose-rich diet (Miksztowicz et al., 2014). Furthermore, Maquoi et al. (2002) reported a decrease in mRNA levels of MMP-9 and no change in mRNA levels of MMP-2 in gonadal adipose tissue of obese mice fed with a HFD for 15 weeks. In accordance, in our study we observed that the HFD group presented a significant decrease in MMP-9 activity compared with the Control group, with no differences in MMP-2 activity. Recently, it has been reported that LGT could modify MMPs expression in different pathologies associated with ECM remodeling (Moustafa et al., 2018; Jia et al., 2021; Meurot et al., 2022). However, to our knowledge, this is the first study showing the effect of LGT on the activity of gelatinases in expanded VAT. We found that LGT promotes an increase in MMP-9 activity accompanied by higher vascular density and lower interstitial fibrosis in HFD VAT. Previous studies have shown that obesity is associated with impaired angiogenesis and augmented fibrosis because of the increase in pro-inflammatory adipokines expression (Lijnen, 2008; Corvera et al., 2022). In adult mice, the higher epididymal fat mass induced by high-fat diets is predominantly at the expense of adipocyte hypertrophy rather than hyperplasia (Jo et al., 2009). Enlarged adipocytes reach the diffusional limit of oxygen leading to hypoxia and stress. Even though this stress is a signal for angiogenesis and ECM remodeling, if the overnutrition is chronic, the tissue continues to expand without being able to adequately enhance angiogenesis. Persistent hypoxia leads to fibrosis and leukocyte recruitment, with the consequential increase in the secretion of pro-inflammatory adipokines and cytokines that promote the systemic metabolic alterations characteristic of obesity. (Crewe et al., 2017). Recently, Zhang et al. (2023) described that LGT regulates angiogenesis in AT by inhibiting IL-6 secretion from adipocytes. Our
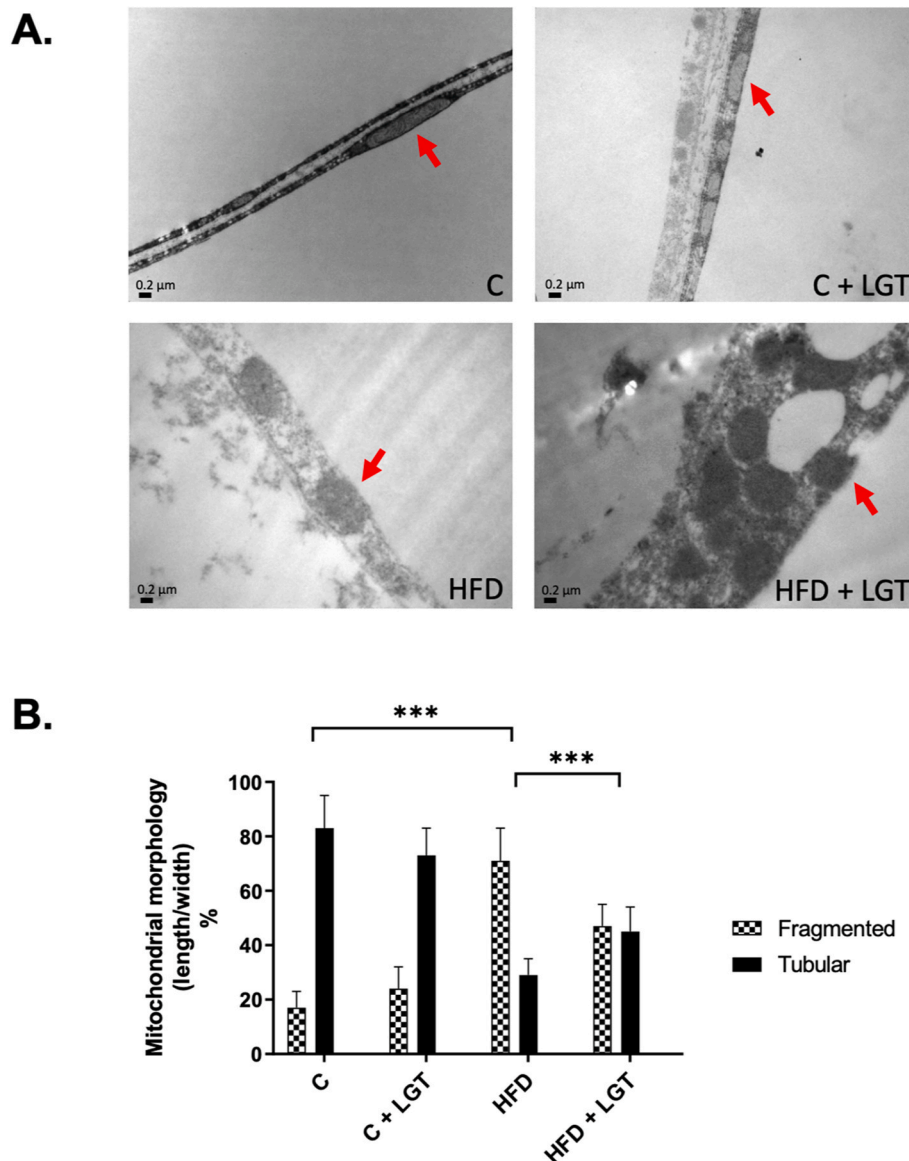
Fig. 6. Analysis of mitochondrial morphology in adipose tissue by transmission electron microscopy. Representative images of mitochondrial morphology by electron microscope images (30.000× magnification). Tubular and fragmented mitochondria were counted per arbitrary area and expressed in percentage. ***$p < 0.001$.

results suggest that activation of MMPs may partially explain the enhancement of VAT vascularization by LGT treatment. In AT, MMPs are synthesized and secreted to the ECM by different cell types, such as adipocytes, fibroblasts, and endothelial cells. Therefore, the increase in MMP-9 activity observed in HFD + LGT could be due to one or more of the following mechanisms: 1) induction of MMP-9 secretion upon these cell types; 2) decreased TIMPs secretion or activity; 3) the increased number of smaller adipocytes observed in this group.

When Gal-3 was investigated, we observed that VAT from HFD presented a lower expression of Gal-3, without changes with LGT treatment. Gal-3 is an important regulator of different biological functions such as cell proliferation, apoptosis, inflammation, and fibrosis, among others. Gal-3 is expressed in several cell types, including adipocytes. Data about its role in VAT remodeling remains controversial due to research showing deleterious and protective effects. Most studies in humans reported that circulating Gal-3 levels are increased in obese and type 2 diabetes patients (Menini et al., 2016; Zeytinli Aksit et al., 2022). Otherwise, animals with Gal-3 deletion showed accumulation of fat mass, inflammation, and altered glucose homeostasis (Pang et al., 2013;

Pejnovic et al., 2013; Blasetti Fantauzzi et al., 2020). In contrast, Baek et al. (2015) reported that Gal-3 knockout mice fed a HFD had significantly lower body weight and VAT compared with wild-type mice. This suggests that Gal-3 is essential for adipocyte differentiation and that its deletion prevents VAT expansion and inflammation. In our study, we observed a positive association between Gal-3 expression and adipocyte number and an inverse correlation with hypertrophic adipocytes. Regarding the effects of LGT, it has been reported that it would reduce Gal-3 levels in the liver of an obese animal model (Tølbøl et al., 2018). However, Simeone et al. (2022) recently reported that LGT treatment did not affect circulating Gal-3 levels in obese patients. In accordance, we did not observe changes in Gal-3 expression in VAT in response to LGT administration. Our data suggests that Gal-3 pathways would not be related to the changes observed in VAT histological characteristics after LGT treatment.

Numerous evidence suggests a link between ECM remodeling and mitochondrial behavior (Yanes and Rainero, 2022). Different studies have described that changes in ECM composition or deposition could affect mitochondrial dynamics (Yapa et al., 2021; Yanes and Rainero,
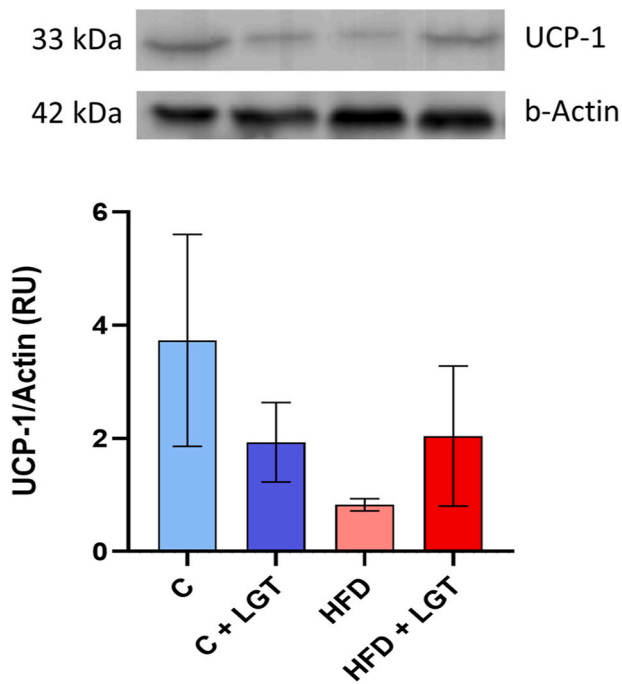
Fig. 7. Quantification of Uncoupling protein-1 (UCP-1) expression in visceral adipose tissue by western blotting. UCP-1 levels in epididymal adipose tissue from Control (C), Control + LGT (C + LGT), HFD and HFD + LGT group. RU, relative units. Data are presented as mean $\pm$ SD.

2022). Mitochondria are organelles whose morphology, density, and distribution reflect metabolic changes. Fission and fusion are processes involved in mitochondrial dynamics. In fission, mitochondria divide into multiple spherical or fragmented structures, whereas in fusion different mitochondria merge to produce tubular organelles. Dysregulation in fission and fusion balance affects mitochondrial behavior, and it has been associated with different pathologies (Yapa et al., 2021). When fission predominates, the increase in spherical mitochondria deteriorates the respiratory process and bioenergetic performance. In our study, animals fed with a HFD showed a prevalence of fragmented mitochondria suggesting a predominant fission process. LGT treatment favored the increase in the proportion of elongated mitochondria, and it would favor thermogenesis through the induction of UCP-1 expression. Our results indicate that in visceral obesity, the histological changes required for VAT expansion affect mitochondrial dynamics; LGT improved mitochondrial density and the balance between spherical and elongated organelles suggesting a possible VAT "browning", a process in which some white adipocytes acquire properties of brown adipocytes. These findings are related to previous research about the beneficial effects of new antidiabetic drugs that activate thermogenic properties in brown adipose tissue (BAT). In an animal model of obesity, it has been recently reported that Tirzepatide, a dual glucose-dependent insulin-tropic polypeptide (GIP) and GLP-1 receptor agonist, would upregulate the expression of genes associated with the catabolism of glucose, lipid, branched-chain amino acids and branched-chain ketoacids in BAT. These direct effects on BAT mimic the effect of cold exposure and would improve insulin sensitization, increase metabolic rate, and weight loss (Samms et al., 2021, 2022).

In this study, the molecular mechanisms through which LGT increases the activity of MMPs and vascularization have not been elucidated. To clarify this point further research is needed. Moreover, it is important to mention that in this study only male mice were studied, given that estrogens modify adipose tissue expansion as well as metabolic profile (Martínez-Cignoni et al., 2021; Moreira-Pais et al., 2020). Furthermore, previous studies suggested that female mice would be protected against HFD-induced metabolic changes while maintaining an anti-inflammatory environment in the intra-abdominal adipose tissue (Pettersson et al., 2012). Different evidence suggests that sex steroids play an essential role in fat distribution, metabolism, proliferation, and function; more research is needed to fully understand the effect of sexual steroids on adipocytes. Indeed, a comparative analysis of the effects of LGT on the remodeling of adipose tissue in males and females should be the focus of future research.

Finally, it has been suggested that including unsaturated fatty acids, such as oleic acid, in the diet can either prevent or postpone the onset of insulin resistance, explaining that animals fed HFD have developed visceral obesity without alterations in insulin resistance markers (Palomer et al., 2018). Hence, it is important to highlight that according to our results, LGT may have effects on expanded VAT even without (or before) systemic insulin resistance. In reference to lipid profile, HFD increased atherogenic lipoproteins levels, even though there were no changes in caloric intake. It is known that lipid levels depend on multiple factors and do not depend only on caloric intake, including the source and amount of fat in the diet, as well as the time of experience. According to previous studies in obese non-diabetic (Ansari et al., 2024) and diabetic patients (Sun et al., 2015; Capehorn et al., 2020), we reported an improvement in lipid profile in obese non-diabetic mice, induced by LGT treatment. Our findings suggest that LGT treatment could prevent cardiovascular disease associated with visceral obesity, through the improvement of lipid profile. This animal model induced by HFD may be useful to further study the cardioprotective effects of LGT in visceral obesity.

Conclusion

In visceral obesity, LGT exerts a beneficial effect on VAT behavior by modulating gelatinase activity and improving vascularization and histological characteristics of adipocytes. In addition, LGT administration improves mitochondrial dynamics and thermogenic factor expression, changes that would favor VAT functionality.

CRediT authorship contribution statement

Vanessa Touceda: Methodology, Validation, Formal analysis, Investigation, Visualization. **Florencia Fontana Estevez:** Methodology, Investigation. **Leonardo Cacciagiú:** Methodology, Investigation. **Paola Finocchietto:** Resources, Formal analysis, Investigation. **Romina Bustos:** Methodology. **Agustina Vidal:** Resources. **Gabriela Berg:** Formal analysis. **Celina Morales:** Methodology. **Germán González:** Writing – review & editing, Funding acquisition. **Veronica Miksztowicz:** Conceptualization, Formal analysis, Investigation, Writing – original draft, Supervision, Project administration, Funding acquisition.

Declaration of competing interest

The authors declare no competing interests.

Data availability

Data will be made available on request.

Acknowledgments

References

Ansari, H.U.H., Qazi, S.U., Sajid, F., Altaf, Z., Ghazanfar, S., Naveed, N., Ashfaq, A.S., Siddiqu, i AH., Iqba, l H., Qaz, i S., 2024. Efficacy and safety of glucagon-like peptide-1 receptor agonists on body weight and cardiometabolic parameters in individuals with obesity and without diabetes: a systematic review and meta-analysis. Endocr. Pract. 30 (2), 160–171. https://doi.org/10.1016/j.eprac.2023.11.007.

Baek, J.H., Kim, S.J., Kang, H.G., Lee, H.W., Kim, J.H., Hwang, K.A., Song, J., Chun, K.H., 2015. Galectin-3 activates PPARγ and supports white adipose tissue formation and high-fat diet-induced obesity. Endocrinology 156 (1), 147–156. https://doi.org/10.1210/en.2014-1374.

Barchuk, M., Miksztowicz, V., Zago, V., Cevey, A., López, G., Goren, N., Friedman, S., Gelpi, R.J., Morale, C., Fernandez Tomé, M.D.C., Schreier, L., Berg, G., 2018. Endothelial lipase is an alternative pathway for fatty acid release from lipoproteins: evidence from a high fat diet model of obesity in rats. Lipids 53 (10), 993–1003. https://doi.org/10.1002/lipd.12107.

Berg, G., Schreier, L., Miksztowicz, V., 2014. Circulating and adipose tissue matrix metalloproteinases in cardiometabolic risk environments: pathophysiological aspects. Horm. Mol. Biol. Clin. Invest. 17 (2), 79–87. https://doi.org/10.1515/hmbci-2013-0069.

Berg, G., Barchuk, M., Miksztowicz, V., 2019. Behavior of metalloproteinases in adipose tissue, liver and arterial wall: an update of extracellular matrix remodeling. Cells 8 (2), 158. https://doi.org/10.3390/cells8020158.

Blasetti Fantauzzi, C., Iacobini, C., Menini, S., Vitale, M., Sorice, G.P., Mezza, T., Cinti, S., Giaccari, A., Pugliese, G., 2020. Galectin-3 gene deletion results in defective adipose tissue maturation and impaired insulin sensitivity and glucose homeostasis. Sci. Rep. 10 (1), 20070 https://doi.org/10.1038/s41598-020-76952-z.

Brinkworth, G.D., Noakes, M., Buckley, J.D., Keogh, J.B., Clifton, P.M., 2009. Long-term effects of a very-low-carbohydrate weight loss diet compared with an isocaloric low-fat diet after 12 mo. Am. J. Clin. Nutr. 90 (1), 23–32.

Capehorn, M.S., Catarig, A.M., Furberg, J.K., Janez, A., Price, H.C., Tadayon, S., Vergès, B., Marre, M., 2020. Efficacy and safety of once-weekly semaglutide 1.0mg vs once-daily liraglutide 1.2mg as add-on to 1-3 oral antidiabetic drugs in subjects with type 2 diabetes (SUSTAIN 10). Diabetes Metab. 46 (2), 100–109. https://doi.org/10.1016/j.diabet.2019.101117.

Cassaglia, P., Penas, F., Betazza, C., Fontana Estevez, F., Miksztowicz, V., Martínez Naya, P., Llamosas, M.C., Noli Truant, S., Wilensky, L., Volberg, V., Cevey, A.C., Touceda, V., Cicale, E., Berg, G., Fernández, M., Goren, N., Morales, C., González, G. E., 2020. Genetic deletion of Galectin-3 alters the temporal evolution of macrophage infiltration and healing affecting the cardiac remodeling and function after myocardial infarction in mice. Am. J. Pathol. 190 (9), 1789–1800. https://doi.org/10.1016/j.ajpath.2020.05.010.

Corvera, S., Solivan-Rivera, J., Yang Loureiro, Z., 2022. Angiogenesis in adipose tissue and obesity. Angiogenesis 25 (4), 439–453. https://doi.org/10.1007/s10456-022-09848-3.

Crewe, C., An, Y.A., Scherer, P.E., 2017. The ominous triad of adipose tissue dysfunction: inflammation, fibrosis, and impaired angiogenesis. J. Clin. Invest. 127 (1), 74–82. https://doi.org/10.1172/JCI88883.

De Cavanagh, EMv, Ferder, M., Inserra, F., Ferder, L., 2009. Angiotensin II, mitochondria, cytoskeletal, and extracellular matrix connections: an integrating viewpoint. Am. J. Physiol. Heart Circ. Physiol. 296 (3), H550–H558. https://doi.org/10.1152/ajpheart.01176.2008.

González, G.E., Rhaleb, N.E., D'Ambrosio, M.A., Nakagawa, P., Liao, T.D., Peterson, E.L., Leung, P., Dai, X., Janic, B., Liu, Y.H., Yang, X.P., Carretero, O.A., 2016. Cardiac-deleterious role of galectin-3 in chronic angiotensin II-induced hypertension. Am. J. Physiol. Heart Circ. Physiol. 311 (15), H1287–H1296. https://doi.org/10.1152/ajpheart.00096.2016.

Heinonen, S., Jokinen, R., Rissanen, A., Pietiläinen, K.H., 2020. White adipose tissue mitochondrial metabolism in health and obesity. Obes. Rev. 21 (2), e12958 https://doi.org/10.1111/obr.12958.

Herold, J., Kalucka, J., 2021. Angiogenesis in adipose tissue: the interplay between adipose and endothelial cells. Front. Physiol. 9 (11), 624903 https://doi.org/10.3389/fphys.2020.624903.

Iepsen, E.W., Torekov, S.S., Holst, J.J., 2015. Liraglutide for Type 2 diabetes and obesity: a 2015 update. Expert Rev. Cardiovasc Ther. 13 (7), 753–767. https://doi.org/10.1586/14779072.2015.1054810.

Jia, Y., Lu, P., Qi, L., Li, J., Wang, M., Qi, J., Song, Y., 2021. Protective roles of liraglutide against brain injury of streptozotocin induced diabetic rats. Pak. J. Pharm. Sci. 34 (6), 2121–2129.

Jo, J., Gavrilova, O., Pack, S., Jou, W., Mullen, S., Sumner, A.E., Cushman, S.W., Periwa, l V., 2009. Hypertrophy and/or hyperplasia: dynamics of adipose tissue growth. PLoS Comput. Biol. 5 (3), e1000324 https://doi.org/10.1371/journal.pcbi.1000324.

Kleiner, D., Stetler-Stevenson, W., 1994. Quantitative zymography: detection of picogram quantities of gelatinases. Anal. Biochem. 218 (2), 325–329. https://doi.org/10.1006/abio.1994.1186.

Levi, Y., Ciaraldi, T., Mudaliar, S., Phillips, S., Henry, R., 2022. Adipose tissue from subjects with type 2 diabetes exhibits impaired capillary formation in response to GROα: involvement of MMPs-2 and -9. Adipocyte 11 (1), 276–286. https://doi.org/10.1080/21623945.2022.2070949.

Li, J., Wu, H., Liu, Y., Yang, L., 2020a. High fat diet induced obesity model using four strains of mice: kunming, C57BL/6, BALB/c and ICR. Exp. Anim. 69 (3), 326–335. https://doi.org/10.1538/expanim.19-0148.

Li, Q.O.Y., Soro-Arnaiz, I., Aragonés, J., 2017. Age-dependent obesity and mitochondrial dysfunction. Adipocyte 6 (2), 161–166. https://doi.org/10.1080/21623945.2017.1297346.

Li, Y.S., Li, X.T., Yu, L.G., Wang, L., Shi, Z.Y., Guo, X.L., 2020b. Roles of galectin-3 in metabolic disorders and tumor cell metabolism. Int. J. Biol. Macromol. 142, 463–473. https://doi.org/10.1016/j.ijbiomac.2019.09.118.

Lijnen, H.R., 2008. Angiogenesis and obesity. Cardiovasc. Res. 78 (2), 286–293. https://doi.org/10.1093/cvr/cvm007.

Liu, Y.T., He, T., Li, H.Q., Jiang, P., 2021. Liraglutide improves pancreatic islet β cell apoptosis in rats with type 2 diabetes mellitus by inhibiting the IKKε/NF-κB pathway. Eur. Rev. Med. Pharmacol. Sci. 25 (14), 4818–4828. https://doi.org/10.26355/eurrev_202107_26395.

Maquoi, E., Munaut, C., Colige, A., Collen, D., Lijnen, H., 2002. Modulation of adipose tissue expression of murine matrix metalloproteinases and their tissue inhibitors with obesity. Diabetes 51 (4), 1093–1101. https://doi.org/10.2337/diabetes.51.4.1093.

Martínez-Cignoni, M.R., González-Vicens, A., Morán-Costoya, A., Proenza, A.M., Gianotti, M., Valle, A., Lladó, I., 2021. Estrogen impairs adipose tissue expansion and cardiometabolic profile in obese-diabetic female rats. Int. J. Mol. Sci. 22 (24), 13573 https://doi.org/10.3390/ijms222413573, 17.

Maughan, R.T., Feeney, E.R., Capel, E., Capeau, J., Domingo, P., Giralt, M., Lange, J.M., Phanuphak, P., Cooper, D.A., Reiss, P., Mallon, P.W., HIVNAT-019 Study Group, 2016. Improved adipose tissue function with initiation of protease inhibitor-only ART. J. Antimicrob. Chemother. 71 (11), 3212–3221. https://doi.org/10.1093/jac/dkw301.

Menini, S., Iacobini, C., Blasetti Fantauzzi, C., Pesce, C.M., Pugliese, G., 2016. Role of galectin-3 in obesity and impaired glucose homeostasis. Oxid. Med. Cell. Longev. 9618092 https://doi.org/10.1155/2016/9618092.

Meurot, C., Martin, C., Sudre, L., Breton, J., Bougault, C., Rattenbach, R., Bismuth, K., Jacques, C., Berenbaum, F., 2022. Liraglutide, a glucagon-like peptide 1 receptor agonist, exerts analgesic, anti-inflammatory and anti-degradative actions in osteoarthritis. Sci. Rep. 12 (1), 1567. https://doi.org/10.1038/s41598-022-05323-7.

Miksztowicz, V., Muzzio, M.L., Royer, M., Prada, M., Wikinski, R., Schreier, L., Berg, G., 2008. Increased plasma activity of metalloproteinase 2 in women with metabolic syndrome. Metabolism 57 (11), 1493–1496. https://doi.org/10.1016/j.metabol.2008.06.001.

Miksztowicz, V., Morales, C., Zago, V., Friedman, S., Schreier, L., Berg, G., 2014. Effect of insulin-resistance on circulating and adipose tissue MMP-2 and MMP-9 activity in rats fed a sucrose-rich diet. Nutr. Metabol. Cardiovasc. Dis. 24 (3), 294–300. https://doi.org/10.1016/j.numecd.2013.08.007.

Miksztowicz, V., Morales, C., Barchuk, M., López, G., Póveda, R., Gelpi, R., Schreier, L., Rubio, M., Berg, G., 2017. Metalloproteinase 2 and 9 activity increase in epicardial adipose tissue of patients with coronary artery disease. Curr. Vasc. Pharmacol. 15 (2), 135–143. https://doi.org/10.2174/1570161114666161024124244.

Milano, W., De Biasio, V., Di Munzio, W., Foggia, G., Capasso, A., 2020. Obesity: the new global epidemic pharmacological treatment, opportunities and limits for personalized therapy. Endocr., Metab. Immune Disord.: Drug Targets 20 (8), 1232–1243. https://doi.org/10.2174/1871530320666200515112853.

Moreira-Pais, A., Ferreira, R., Neves, J.S., Vitorino, R., Moreira-Gonçalves, D., Nogueira-Ferreira, R., 2020. Sex differences on adipose tissue remodeling: from molecular mechanisms to therapeutic interventions. J. Mol. Med. (Berl.) 98 (4), 483–493. https://doi.org/10.1007/s00109-020-01890-2.

Moustafa, P., Abdelkader, N., El Awdan, S., El-Shabrawy, O., Zaki, H., 2018. Liraglutide ameliorated peripheral neuropathy in diabetic rats: involvement of oxidative stress, inflammation and extracellular matrix remodeling. J. Neurochem. 146 (2), 173–185. https://doi.org/10.1111/jnc.14336.

Nauck, M.A., Quast, D.R., Wefers, J., Meier, J.J., 2021. GLP-1 receptor agonists in the treatment of type 2 diabetes - state-of-the-art. Mol. Metabol. 46, 101102 https://doi.org/10.1016/j.molmet.2020.101102.

National Research Council, 2012. Guide for the Care and Use of Laboratory Animals, eighth ed. The National Academies Press. https://doi.org/10.1258/la.2012.150312.

Palomer, X., Pizarro-Delgado, J., Barroso, E., Vázquez-Carrera, M., 2018. Palmitic and oleic Acid: the yin and yang of fatty acids in type 2 diabetes mellitus. Trends Endocrinol. Metabol. 29 (3), 178–190. https://doi.org/10.1016/j.tem.2017.11.009.

Pang, J., Rhodes, D.H., Pini, M., Akasheh, R.T., Castellanos, K.J., Cabay, R.J., Cooper, D., Perretti, M., Fantuzzi, G., 2013. Increased adiposity, dysregulated glucose metabolism and systemic inflammation in galectin-3 KO mice. PLoS One 8 (2), e57915. https://doi.org/10.1371/journal.pone.0057915.

Pejnovic, N.N., Pantic, J.M., Jovanovic, I.P., Radosavljevic, G.D., Milovanovic, M.Z., Nikolic, I.G., Zdravkovic, N.S., Djukic, A.L., Arsenijevic, N.N., Lukic, M.L., 2013. Galectin 3 deficiency accelerates high-fat diet-induced obesity and amplifies inflammation in adipose tissue and pancreatic islets. Diabetes 62 (6), 1932–1944. https://doi.org/10.2337/db12-0222.

Pettersson, U.S., Waldén, T.B., Carlsson, P.O., Jansson, L., Phillipson, M., 2012. Female mice are protected against high-fat diet induced metabolic syndrome and increase the regulatory T cell population in adipose tissue. PLoS One 7 (9), e46057. https://doi.org/10.1371/journal.pone.0046057.

Piché, M.E., Tchernof, A., Després, J.P., 2020. Obesity phenotypes, diabetes, and cardiovascular diseases. Circ. Res. 126 (11), 1477–1500. https://doi.org/10.1161/CIRCRESAHA.120.316101.

Powell-Wiley, T.M., Poirier, P., Burke, L.E., Després, J.P., Gordon-Larsen, P., Lavie, C.J., Lear, S.A., Ndumele, C.E., Neeland, I.J., Sanders, P., St-Onge, M.P., 2021. American heart association Council on lifestyle and cardiometabolic health; Council on cardiovascular and stroke nursing; Council on clinical cardiology; Council on epidemiology and prevention; and stroke Council. Obesity and cardiovascular disease: a scientific statement from the American heart association. Circulation 143 (21), e984–e1010. https://doi.org/10.1161/CIR.0000000000000973.

Raja, V., Aguiar, C., Alsayed, N., Chibber, Y.S., ElBadawi, H., Ezhov, M., Hermans, M.P., Pandey, R.C., Ray, K.K., Tokgözoglu, L., et al., 2023. Non-HDL-cholesterol in

dyslipidemia: review of the state-of-the-art literature and outlook. Atherosclerosis 383, 117312. https://doi.org/10.1016/j.atherosclerosis.

Sahakyan, K.R., Somers, V.K., Rodriguez-Escudero, J.P., Hodge, D.O., Carter, R.E., Sochor, O., Coutinho, T., Jensen, M.D., Roger, V.L., Singh, P., et al., 2015. Normal-weight central obesity: implications for total and cardiovascular mortality. Ann. Intern. Med. 163, 827–835. https://doi.org/10.7326/M14-2525.

Samms, R.J., Christe, M.E., Collins, K.A., Pirro, V., Droz, B.A., Holland, A.K., Friedrich, J. L., Wojnicki, S., Konkol, D.L., Cosgrove, R., et al., 2021. GIPR agonism mediates weight-independent insulin sensitization by tirzepatide in obese mice. J. Clin. Invest. 131 (12), e146353 https://doi.org/10.1172/JCI146353.

Samms, R.J., Zhang, G., He, W., Ilkayeva, O., Droz, B.A., Bauer, S.M., Stutsman, C., Pirro, V., Collins, K.A., Furber, E.C., et al., 2022. Tirzepatide induces a thermogenic-like amino acid signature in brown adipose tissue. Mol. Metabol. 64, 101550 https://doi.org/10.1016/j.molmet.2022.101550.

Simeone, P., Tripaldi, R., Michelsen, A., Ueland, T., Liani, R., Ciotti, S., Birkeland, K.I., Gulseth, H.L., Di Castelnuovo, A., Cipollone, F., Aukrust, P., Consoli, A., Halvorsen, B., Santilli, F., 2022. Effects of liraglutide vs. lifestyle changes on soluble suppression of tumorigenesis-2 (sST 2) and galectin-3 in obese subjects with prediabetes or type 2 diabetes after comparable weight loss. Cardiovasc. Diabetol. 21 (1), 36. https://doi.org/10.1186/s12933-022-01469-w.

Sun, F., Wu, S., Wang, J., Guo, S., Chai, S., Yang, Z., Li, L., Zhang, Y., Ji, L., Zhan, S., 2015. Effect of glucagon-like peptide-1 receptor agonists on lipid profiles among type 2 diabetes: a systematic review and network meta-analysis. Clin. Therapeut. 37 (1), 225–241. https://doi.org/10.1016/j.clinthera.2014.11.008 e8.

Tamura, K., Minami, K., Kudo, M., Iemoto, K., Takahashi, H., Seino, S., 2015. Liraglutide improves pancreatic Beta cell mass and function in alloxan-induced diabetic mice. PLoS One 10 (5), e0126003. https://doi.org/10.1371/journal.pone.0126003.

Tinahones, F.J., Coin-Araguez, L., Mayas, M.D., García-Fuentes, E., Hurtado Del Pozo, C., Vendrell, J., Cardona, F., Calvo, R.M., Obregon, M.J., Bekay, R.E., 2012. Obesity-associated insulin resistance is correlated to adipose tissue vascular endothelial growth factors and metalloproteinase levels. BMC Physiol. 12 (4) https://doi.org/10.1186/1472-6793-12-4.

Tølbøl, K.S., Kristiansen, M.N., Hansen, H.H., Veidal, S.S., Rigbolt, K.T., Gillum, M.P., Jelsing, J., Vrang, N., Feigh, M., 2018. Metabolic and hepatic effects of liraglutide, obeticholic acid and elafibranor in diet-induced obese mouse models of biopsy-confirmed nonalcoholic steatohepatitis. World J. Gastroenterol. 24 (2), 179–194. https://doi.org/10.3748/wjg.v24.i2.179.

Wołosowicz, M., Łukaszuk, B., Kasacka, I., Chabowski, A., 2022. Diverse impact of N-acetylcysteine or alpha-lipoic acid supplementation during high-fat diet regime on matrix metalloproteinase-2 and matrix metalloproteinase-9 in visceral and subcutaneous adipose tissue. Cell. Physiol. Biochem. 56 (2), 166–179. https://doi.org/10.33594/000000511.

Yanes, B., Rainero, E., 2022. The Interplay between cell-extracellular matrix interaction and mitochondria dynamics in cancer. Cancers 14 (6), 1433. https://doi.org/10.3390/cancers14061433.

Yapa, N.M.B., Lisnyak, V., Reljic, B., Ryan, M.T., 2021. Mitochondrial dynamics in health and disease. FEBS Lett. 595 (8), 1184–1204. https://doi.org/10.1002/1873-3468.14077.

Zeytinli Aksit, M., Demet Arslan, F., Karakoyun, I., Aydin, C., Turgut, E., Parildar, H., Gokbalci, U., Isbilen Basok, B., Duman, C., Emiroglu, M., 2022. Galectin-3 levels and inflammatory response in patients undergoing bariatric surgery. Cytokine 151, 155793. https://doi.org/10.1016/j.cyto.2022.155793.

Zhang, R., Yao, K., Chen, S., Pan, X., Wu, F., Gao, P., 2023. Liraglutide promotes angiogenesis in adipose tissue via suppression of adipocyte-derived IL-6. Biochem. Biophys. Res. Commun. 651, 8–19. https://doi.org/10.1016/j.bbrc.2023.02.007.